ROBOTICS AND MECHATRONICS

NON-INVASIVE SENSING MECHANISMS FOR SOFT PNEUMATIC ACTUATORS IN INTELLIGENT ROBOTIC ENDOSCOPES

S. (Srisaran) Arul Anand

MSC ASSIGNMENT

Committee:
dr. ir. M. Abayazid
M.A.A. Atalla, MSc
V.R. Puranam, MSc
dr. ir. A.Q.L. Keemink

March, 2025

013RaM2025
Robotics and Mechatronics
EEMCS
University of Twente
P.O. Box 217
7500 AE Enschede
The Netherlands

UNIVERSITY OF TWENTE. | TECHMED CENTRE
UNIVERSITY OF TWENTE. | DIGITAL SOCIETY INSTITUTE

Acknowledgment

I sincerely thank my supervisor, Momen Abayazid. Since day one, he structured my path towards my end goal. He makes himself available even during his busy schedule to guide me. He is a humble person who appreciates me and gave consistent support throughout my thesis. I learned the right procedure to conduct research without immersing myself deeply in a specific problem. I deeply thank him for his continuous support throughout my thesis.

Next, my daily supervisor Rithwick Puranam joined a bit late in my thesis. I could have done much faster and even better if he had traveled with me from day one. He perfected me with minute details. I learned a lot about data analysis and presentation skills necessary for my weekly meetings. I got better at expressing my results in the meetings. I am immensely grateful for his constant support and guidance.

Next, I thank Mostafa Atalla, for his guidance during my thesis. He showed the correct way of conducting experiments and proper way to present my report.

My sincere gratitude goes to Marijon Kuipers for helping with fabrication. She was always available even during her busy schedule, and I am grateful to her. Next, Gijs van Oort was my go-to person for understanding sensors and microcontrollers. He has excellent knowledge and experience in this field. He made me solve all the puzzles, which were interesting and tricky. I am incredibly thankful for his constant support during difficult times. Next, Sander Smits helped me with small technical details I needed to catch up on. I am thankful for his support. Next, I am grateful to Artur Gasienica for helping me to with rapid prototyping 3D molds.

Next, I am grateful to have lovely friends and family who were my constant throughout my master's. Few made me realize who I am and were there to cheer and back me up. I extend my special thanks to my mom, who supported me. I extend my appreciation to ChatGPT for its assistance in refining and enhancing the clarity of my report. I thank everyone who was there for me throughout my thesis.

Abstract

Minimally Invasive Surgery (MIS) is an advanced medical procedure performed through small incisions with specialized tools and advanced technologies. Compared to conventional open surgery, MIS reduces physical trauma by reducing the size and number of incisions. These procedures require intelligent robotic endoscopes (IRE's) with autonomous maneuvering capabilities, offering sensory feedback beyond traditional endoscopes. A Soft Pneumatic Actuator (SPA) serves an IRE but suffer performance issues when embedded with physical sensors. This thesis aims to establish a sensing mechanism without involving physical sensors on the soft pneumatic actuator. SPA possesses intrinsic sensing capabilities, When a pneumatic actuator interacts with its surroundings, the volume of the SPA changes to external interaction. These interactions can be quantified using external pressure sensors. So the pressure sensor data's collected in the time domain is converted into the frequency domain for analysis. This thesis examines the relationship between pressure, volume, phase shift and external forces acting on the soft pneumatic actuator. A stronger correlation between phase shift, external forces and volume are absorbed in experimental results. Additionally, the soft actuators exhibit varying external forces due to non-linearities and it is reflected in varying phase shifts. The findings conclude that pressure, phase shift and external forces acting on the SPA are directly proportional. Additionally, a simple linear regression model was developed, achieving a root mean square error (RMSE) of 0.024 N.

Contents

List of Figures

List of Tables

1 Introduction

Minimally invasive surgery (MIS) are advanced surgical techniques performed through small incisions reducing body trauma compared to traditional open surgeries. MIS provides patients with shorter hospital stays, lower risk of infection, and fewer postoperative complications [1]. However, open surgery have fewer advantages: direct visibility, flexibility, versatility, and easier management of complications [2]. These advantages can be addressed using advanced technologies for MIS applications. Such as, Endoscopes provides visual aid of the surgical area for precise operation, helps to identify internal bleeding and provide direct access to the surgical site.

An endoscope is a medical instrument that helps to look deeper into the body. There are two types of endoscope: rigid and flexible. The flexible endoscope suits better for Gastrointestinal (GI) Surgical Procedures [1]. Traditional flexible endoscopes are human-operated; the practitioners manually insert the endoscope through natural orifices. The tip of the endoscope is controlled using manual rotational knobs, making manual insertion of the endoscope without sensory feedback is both unsafe and time-consuming. Even today, doctors rely on visual assessment to predict area of interest and take multiple biopsies. Most of the time, biopsies are taken close to the area of interest, making the process iterative and requiring a lot of time and effort [3]. Hence, to improve precision and safer operation, an intelligent robotic endoscope (IRE) is recommended.

An IRE integrates actuators and sensory feedback for enhanced navigation and accuracy. Actuators facilitate powered motion, while sensory feedback ensures precise maneuvering. One of the most effective ways to achieve this is through soft pneumatic actuators (SPAs), which rely on pneumatic actuation for its movement. Since SPA operates in an undefined environment, integrating force feedback into the system provides safer and efficient control. [4].

However, implementing force feedback in (SPAs) is challenging due to their hyper-elastic nature. Direct integration of physical sensors, within the SPA restrict the actuator expansion. To prevent such limitations, this thesis explores an alternating sensing mechanism to estimate the external force exerted on the SPA, using external pressure sensors.

1.1 Research question

Estimating external forces on Soft Pneumatic Actuators poses challenges, particularly in integrating physical sensors. The literature review suggests that non-invasive methods offer an alternative approach for estimating forces acting on the actuator. Hence, the study aims to address: “How can internal pressure variations on soft pneumatic actuator (SPA) can be used for external force estimation on actuator? ”

1. “Do intrinsic characteristics of SPA affect the external force estimation? ”
2. “What is the effect of non-linearities on external force estimation? ”
3. “How does a change in volume affect the external forces acting on the actuator?”

1.2 Thesis Outline

In this chapter, SPAs were introduced, raising the question of other efficient ways of sensing. Chapter 2 provides a detailed literature review on SPA, pressure sensors, and the critical pressure-volume hypothesis. Chapter 3 details the materials and methods and experimental setups. Next, various results are compared in the Chapter 4, and discussed in the Chapter 5 and the Chapter 6 provides a conclusion and recommendation.

2 Literature review

This part of the chapter explores the existing literature on establishing a relationship between intrinsic properties of SPA.

2.1 Background

An endoscope is a diagnostic tool for visualizing internal organs, cavities, or body parts. There are two types of endoscopes: rigid and flexible. The rigid endoscope is stiff and mostly used for precise visualization of specific body part [1]. Small incisions are made in laparoscopic surgeries, and the rigid endoscope is inserted for direct visualization. However, its rigidity makes it less suitable for irregular pathways. Hence, MIS require both rigid and flexible endoscopes.

A flexible endoscope consists of a long, thin, and flexible tube with a camera, light source, air channel, and water spray at the end effector. The Figure 2.1 (a) illustrates the structure of flexible endoscope. Normally, a gastroscope is inserted through the natural orifices, which travel through the esophagus and stomach and can reach up to the duodenum of the small intestine. The end effector of this endoscope is controlled using a rotating knob; practitioners are required to use both hands for its operation. However, due to manual insertion, the endoscope's are wrongly inserted into windpipe, causing discomfort and suffocation for the patients. Additionally, it curves around in unintended ways making navigation difficult for the operator. Furthermore, traditional flexible endoscopic operation requires at least 3-4 medical workers.

To overcome these issues, a robotic endoscope is needed for safer and more precise diagnosis. Equipped with actuators and sensors, it can move and navigate efficiently, reducing risks for both patients and doctors. This advancement is especially crucial for advanced surgical operation like Minimally Invasive Surgeries (MIS), enhancing precision and patient safety.

One of the promising approach is the Soft Pneumatic Actuator, which operates with pneumatics. STIFF-FLOP module is a notable example, of a soft pneumatic endoscope specially designed for MIS applications. It is made up of silicone, a bio-compatible material that is gentler on internal tissues, reducing risk of internal damage compared to traditional flexible endoscopes. Here, pneumatic power replaces the manual insertion of the endoscope. The STIFF-FLOP actuator consists of three pneumatic chambers. Enabling omni directional motion as a replacement for the rotating knob in traditional endoscopes [5]. Since STIFF-FLOP module was specially designed for colonoscopy, it had a external diameter of 25 mm. however, as the key focus of this thesis is gastroscopy, a fibre-reinforced SPA is preferred,as a gastroscope should have a maximum diameter of 12 mm [6] [7].

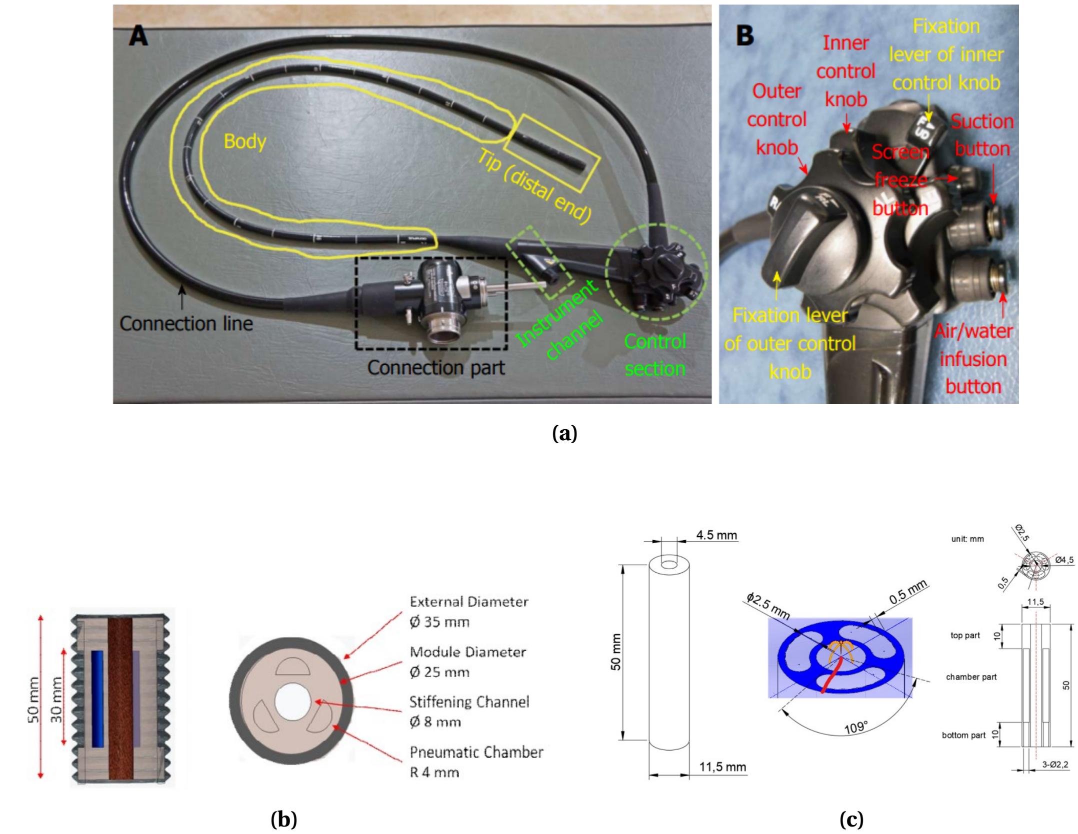

Figure 2.1: (a) Traditional flexible endoscope [3] (b) STIFF-FLOP module [8] (c) Fibre reinforced SPA module [6][7]

2.2 Intrinsic property of SPA

Soft robots are delicate and often designed to interact safely in unknown environments and it requires flexible and stretchable sensors demanding complex integration with SPA [9]. However, soft robots themselves possess intrinsic sensing capabilities, which means their compliance and internal chamber volume change when they interact with the surroundings [10]. We could use these properties to estimate the external forces acting on the actuator. Hence, a complete understanding of the geometric and mechanical properties of the actuator are required.

2.3 STIFF-FLOP

STIFF-FLOP is a SPA designed for colonoscopy. Figure 2.1 (b) represents STIFF-FLOP module. It was designed based on a modular architecture with MRI compatibility. It is made from soft silicon (Ecoflex 00-50 smooth-On), a flexible hyper elastic material that allows changes in the material's stiffness [11]. It has a dedicated central chamber for granular jamming; it stiffens when the vacuum is applied. Since elastic materials are isotropic, there are no preferential directions of expansion; here, an external braid is used, which restricts radial expansion and allows longitudinal elongation.

STIFF-FLOP has three semi-circular pneumatic chambers internally arranged at 120 degrees. External pneumatic valves control the actuator. Simultaneous actuation of a single chamber or two chambers allows omnidirectional bending and elongates when inflating all three chambers [2]. The chambers in the STIFF-FLOP module expand radially up to 0.3 bar and cause a slow

Part	Material	Young's modulus
Chamber part	Eco-flex 0050	12 psi
Top part	Dragon skin 10	22 psi
bottom part	Dragon skin 10	22 psi
Center part	Dragon skin 10	22 psi

Table 2.1: Material properties of fibre reinforced SPA

increase in the bending angle. Next, after 0.3 bar, the external braid restricts radial expansion and improves bending. Then, at 0.55 bar, the increase rate attains saturation because of the external braid [11]. The STIFF-FLOP maximum single chamber bending angle is 120 degrees, with the maximum external force by a single chamber 24.6 N at a pressure of 0.65 bar.

2.4 Fibre reinforced SPA

Fibre reinforced SPA is a reconstructed STIFF-FLOP module for endoscopic applications. The design features remain similar, such as three- semi-circular pneumatic chambers internally arranged at 120 degrees. However, the key difference comes in the characteristics of the module. The fibre reinforced SPA module has an external diameter of 11.5 mm, whereas the STIFF-FLOP has an external diameter of 35 mm as shown in the Figure 2.1 (b). Next, the fibre reinforced SPA and did not have granular jamming because of space constraints. The semi-circular chambers are replaced with bean-shaped chambers, which increases the internal chamber area. These are the key differences STIFF-FLOP and fibre reinforced SPA [6] [7]. Figure 2.1 (C) depicts fibre reinforced SPA.

The soft pneumatic actuator is 50 mm long; it has three internal pneumatic chambers arranged at 120 degrees, similar to the STIFF-FLOP module. The bottom, top, and central chamber are made of dragon skin 10. The pneumatic chambers are made up of (Ecoflex 00-50). The thickness of the wall with the chamber is 0.5mm. The chamber dimension is 2.5 mm in diameter. In this thesis, this fibre reinforced SPA is used.

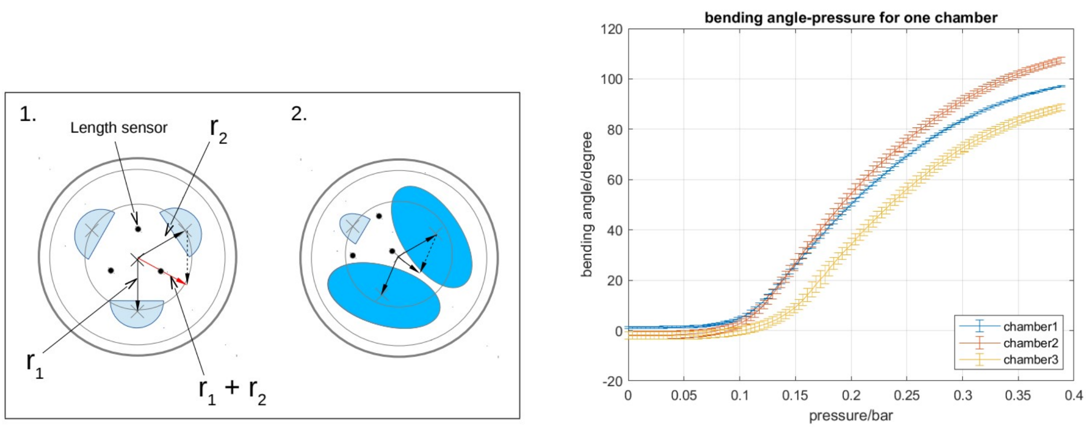

(a) **(b)**

Figure 2.2: (a) Internal chamber expansion [8] (b) Bending angle of SPA [6]

Characteristics	Value	material
Length of actuator	50 mm	Eco-Flex, dragon skin 10
Actuator diameter	11.5 mm	Eco-Flex, dragon skin 10
length of actuator	30 mm	Eco-Flex, dragon skin 10
Top part	10 mm	dragon skin 10
bottom part	10 mm	dragon skin 10
wall thickness	0.5 mm	Eco-Flex
wall thickness	0.5 mm	Eco-Flex
Cross-sectional area of single chamber	17.6 mm^2	
moment of inertia	1717.083 mm^4	
volume of chamber	528 mm^3	

Table 2.2: Structural properties of fibre reinforced SPA

2.5 Characterization

This part of chapter describes a detailed characterization of the fibre reinforced SPA. This includes structural and geometric characterization.

2.5.1 Structural properties

Figure 2.1 (c) represents the front view, top view, and structure of internal chambers. The length, external radius, and central chamber diameter are represented in the front view. The top view represents the chamber alignment; the internal chamber structure represents the chamber internal figure. A detailed structural properties are given in table 2.2. Next, when the actuator is inflated, it expands in the inward direction, as shown in the Figure 2.2 a. The inward inflation is because of the external braid. So, because of this inflation, undesirable effects are caused in the geometry of the actuation, leading to nonlinear actuation and model complications. Next, internal inflation is not uniform because of multiple chambers and external braid, which results in nonlinear behavior [11]. When pressure is applied to a SPA, the geometric center of the chamber moves towards the center of the module. This is pictorially represented in the Figure 2.2 a. Next, actuation energy is wasted by friction between the external silicon surface and the external braid, affecting the desired chamber elongation. When a single chamber is pressurized, it expands and increases cross-section of the chamber.

2.5.2 Geometric properties

Bending moment: When a soft pneumatic actuator is pressurized, the actuator deforms. The bending moment describes the rotational force exerted by the actuator. The force acting in each cross-section can be described as :

$$F_{ext} = PA \tag{2.1}$$

The force in each cross-section is parallel to the z-axis, so the moment around the z-axis is zero. Next, a constant bending moment is expected as the chamber diameter and pressure are assumed constant throughout the module.

$$\vec{M} = \vec{r} \times \vec{F_{ext}} \tag{2.2}$$

This equation fits well for a single chamber expansion. In the above equation, vector $\vec{r}$ represents a vector from the chamber's center. The force F_{ext} is the internal force due to induced pressure. The above figure shows its pictorial view.

Next for 2 chamber expansion,

$$\vec{M} = (\vec{r}_1 + \vec{r}_2) \times \vec{F} \tag{2.3}$$

When 0.5 bar of pressure is applied to it, a maximum of 120 degrees is obtained. Almost all the chambers have similar bending angles. Figure 2.2 (b) shows that single-chamber bending and two-chamber bending provide similar bending. Hence, the geometric properties play a important role in understanding behavior of the actuator. The table 2.3 provides the geometric properties of fibre reinforced SPA.

Symbol	Meaning	value
E	Young's modulus	0.0827 N/mm^2
A	Cross-section area of single arc chamber	17.6 mm^2
A'	Cross-section area of the silicon part	35.16 mm^2
r	length of vector	12mm
l	Length of module	50mm
I	Second moment of inertia	1717.083 mm^4

Table 2.3: Geometrical characteristics of fibre reinforced SPA

Only a few studies have been conducted to understand the relationship between pressure, volume, displacement, and external forces of SPA. In one of the interesting papers, a rigid gripper with antagonistic chambers was embedded in a hybrid gripper to estimate the object's stiffness and contour without using dedicated sensors. The results prove the inherent relationship between those properties [9]. Figure 2.3 (b) depicts the antagonistic actuator setup. Since the antagonistic chambers exhibit one degree of freedom, the relationship between pressure and volume in [9] could be restricted to a single dimension.

Next, intrinsic characteristics of soft actuators were studied in [10]. A compact exo-suit was equipped with soft pneumatic actuators to enhance its comfort and adaptability. The SPA was powered with a constant flow Pneumatic Supply System (PSS) [12]. The soft pneumatic pack consists of 4 pneumatic actuators that are serially arranged. The research used pressure sensors to estimate external forces acting on the soft pneumatic pack.

The soft pneumatic pack Figure 2.3 (c) works similarly to the (fibre reinforced SPA) module: SPA pack has a active chamber and buckles when it is actuated. The actuator was tested in two experimental setups to determine a relationship between pressure and volume. The actuator's motion and external forces acting on it were restricted in the experiments.

Before the experiments, the flow rate of the pneumatic actuator was experimentally obtained using a flow sensor, and a non-linear function was created to remove the dependence of the flow sensor in the circuit. The pressure sensors obtained the relationship between pressure, volume, displacement, and external force acting on the actuator. The measurements were in the time domain.

2.6 Sensor-less estimation of SPA

Figure 2.3 (a) depicts the pressure and volume relationship. The blue curve indicates the free expansion of SPA, where the volume of the actuator increases with increasing pressure. On the other hand, when the actuator is blocked, the volume of the actuator does not increase concerning the increase in pressure. In Figure 2.3 (a) blue ramp represents free volume ex-

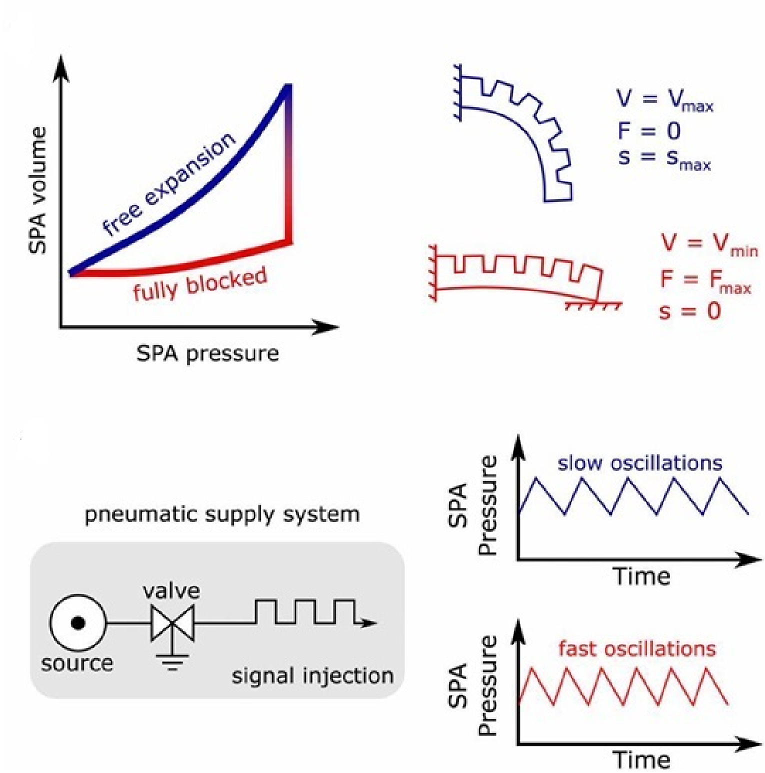

(a)

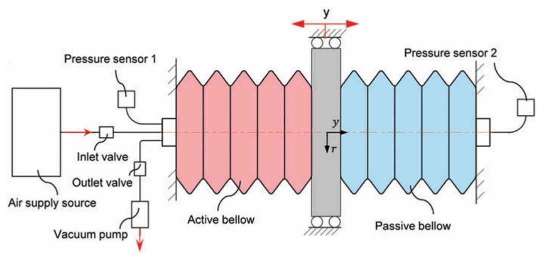

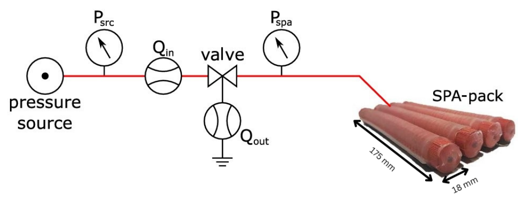

(b) **(c)**

Figure 2.3: (a) Sensor less- Estimation of SPA [10] (b) Antagonistic actuator setup [9] (c) Exo suit SPA setup [10]

pansion, and the red ramp indicates fully blocked volume expansion: when the SPA expands freely, slow oscillations are observed. On the other hand, When it is blocked, faster oscillations are observed. This frequency changes were used to estimate the relationship between pressure, volume, force and displacement. The exo-suit experiment used a constant flow Pneumatic supply system (PSS) as shown Figure 2.3 (c). They used two pressure sensors in their experiments and a single-layer neural network to estimate the relationship in time domain [10].

However, the fiber reinforced SPA module prefers a constant pressure PSS to precisely control the SPA. So, thesis only uses the modified concept provided in the Figure 2.3 (a). Since frequency changes were not visible in time and frequency domain. On further research [13] suggest that, free expansion has greater phase shift compared to constrained expansion. So a new relationship between spa volume and pressure were established using Phase shifts between the pressure sensors, to estimate external force estimation.

3 Materials and methods

This chapter describes the experimental framework of characterization and force tests. These experiments validate the concept and its compatibility on Soft Pneumatic Actuator (SPA).

3.1 Study objective

Here, we conducted characterization and force tests experiments. The aim of the characterization experiment is to verify and validate the hypothesis from section 2. In this experiment, we excite single pneumatic chamber and monitor the pressure differences free expansion. Next, we examine the relationship in constrained expansion. Next, we conducted a force experiments to estimate the external forces acting on the actuator. The purpose of this experiment was to validate the hypothesis against load cell.

3.2 Approach

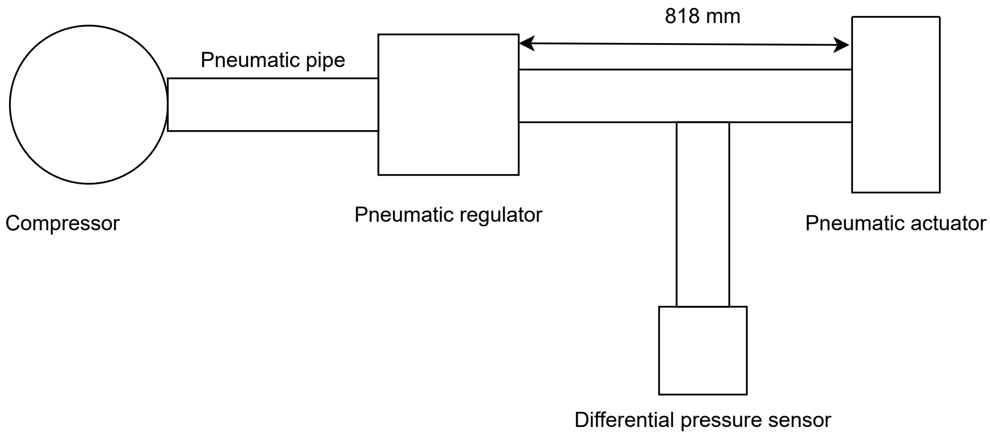

Figure 3.1: Schematic diagram of experimental setup

In this thesis, we aim to establish a relationship between the phase shift and external force acting on the actuator. With the help of two pressure sensors we are estimating the phase shift between them. Figure 3.1 illustrates the schematic of our experimental setup, which consists of two pressure sensors, one positioned at the pneumatic regulator and other near the Pneumatic actuator.

For the experiment, a single chamber is actuated using a 10 Hz sinusoidal pressure through the pneumatic regulator. During free expansion, the air flows from the pneumatic regulator, and actuator expands freely. In this case internal volume of the chamber increases, creating additional volume in the system. In contrast, during constrained expansion, SPA is blocked restricting chamber expansion. We propose that the time required for pressurized air to travel from pneumatic regulator is longer in free expansion compared to constrained expansion. To validate this hypothesis, experiments were conducted in this thesis.

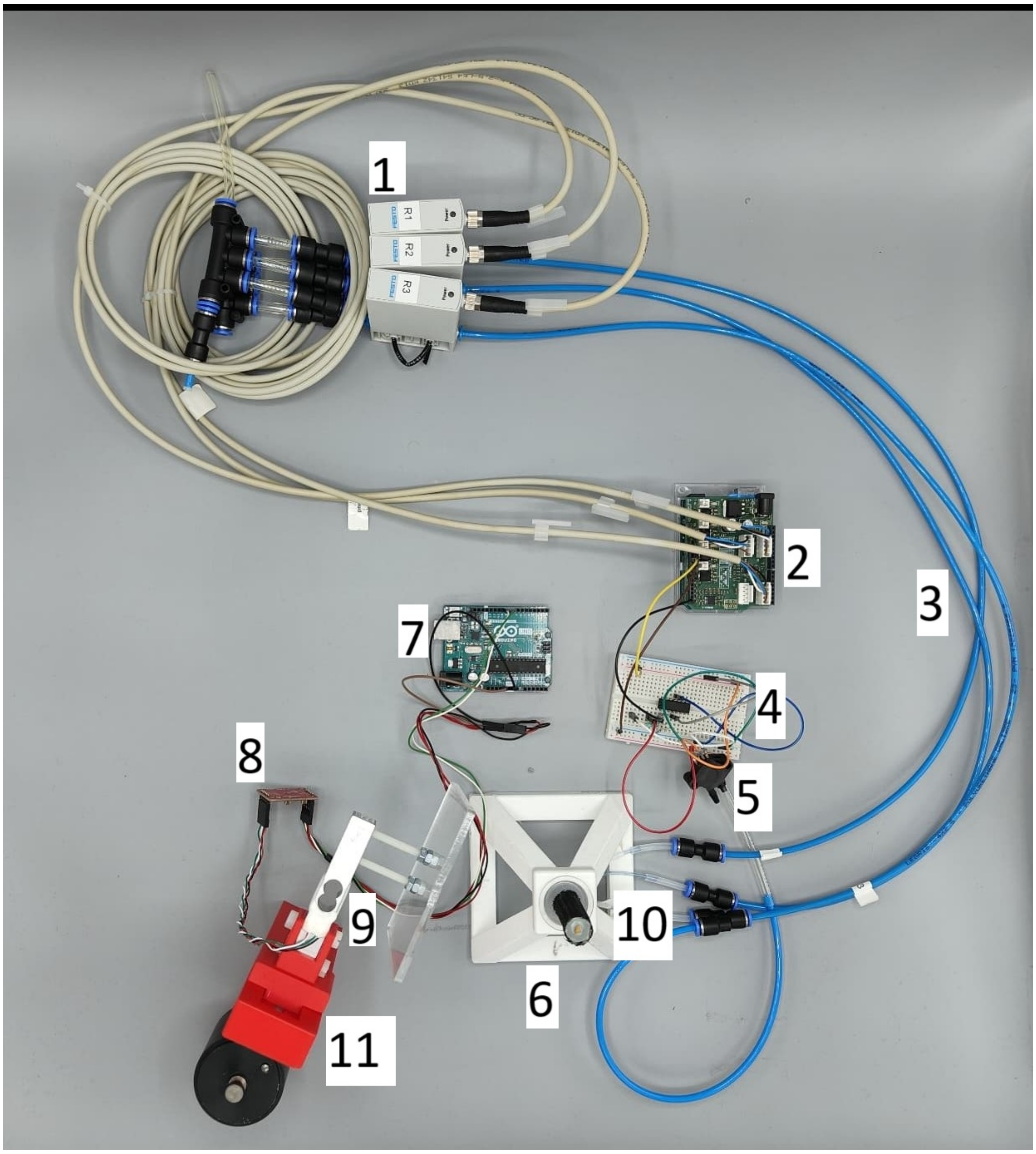

Figure 3.2: Experimental setup - (1) Pneumatic regulator, (2) Pneumatic driver shield, (3) Pneumatic pipe, (4) Pressure sensor ADC , (5) Differential pressure sensor, (6) Pneumatic regulator stand, (7) Arduino Uno, (8) HX711 ADC, (9) Load cell, (10) Fibre reinforced SPA, (11) Load cell stand

3.3 Materials

This section provides a detailed explanation of the experimental setup used in this thesis. All the experiments use a similar setup, with the addition of a few sensors.

Here, we use a proportional pressure regulator (Festo VEAB-L-26-D13-Q4-A4-1R1). It is represented in the Figure 3.2 (1). It is a precise pneumatic control valve with an inbuilt pressure sensor. This pneumatic pressure sensor is an analog sensor with high precision and accuracy. It has internal filters, which reduce the signal-to-noise ratio. The regulator consists of three working ports. Port port 1 is the pneumatic positive pressure port, and port 3 is the vacuum or exhaust port. The port two is connected to the soft pneumatic actuator. The regulator requires a stable 24 V for its operation. It has a working range from -1 bar to 1 bar. The nominal flow rate is around 17 L/min. Here, we use Arduino Uno to control, pneumatic regulator. Since the Arduino Uno works with a standard 5V, an external pneumatic driver shield is used for the regulator's power requirements.

Arduino Uno is a microcontroller with an ATmega328P MCU microprocessor. It is represented in the Figure 3.2 (2). It works with clock speeds up to 16 MHz, which would be sufficient for the operation. Since a constant 24 V is required for regulator, a pneumatic driver shield is used to integrates Arduino UNO and pneumatic pressure regulator.

Next, we use (MPX2050DP) is a Piezo-resistive differential pressure sensor. It is represented in the Figure 3.2 (5). where pressure changes are directly proportional to the change in piezo resistance. It works in the range of 0 - 0.5 bar. Next, the sensor has a sensitivity of 0.8 mV/Kpa, which is an ideal requirement for the setup. This sensor outputs 40mv. So, a differential amplifier setup is used in these experiments. The differential amplifying circuit of few resistors, a voltage amplifier (LM324). It is represented in the Figure 3.2 (4)
Next, a parallel beam load cell (TAL 220) is used to estimate the external forces acting on the actuator. It is represented in the Figure 3.2 (9). The load cell consists of four resistive strain gauges which provide accurate forces. The load cell connected to (HX711) ADC converter. It is a 24-bit ADC converter, which provides precise output weight. It is represented in the Figure 3.2 (8).

3.4 Control system

During the experiments, constant air leakage was observed. To address this issue, a simple feedback loop was created, as shown in Figure 3.3, to maintains optimal pressure in the system. Due to these leakages, the mean pressure dropped to 0.175 bar instead of 0.2 bar. This simple feedback loop was implemented in simulink Matlab.

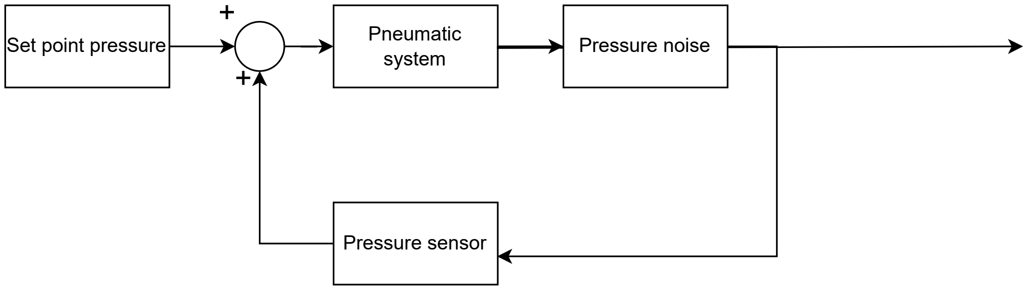

Figure 3.3: Feedback control loop to compensate pressure losses

3.5 Experimental setup

This part of the report provides a broader research perspective and a step-by-step approach to the experiments. An experimental setup is crucial to identifying the relationship between pressure and SPA volume. In this setup, we use two pneumatic pressure sensors. One comes with the Festo pneumatic regulator, and another (differential pressure sensor) is placed near the actuator. When a sinusoidal pressure is applied, the pneumatic air travels through this long blue pneumatic pipe (733 mm), as shown in Figure 3.2 (3). Then, the two-way splitter splits the pneumatic air into an actuator and pressure sensor. The length from the splitter to the actuator is 85 mm. So, when air travels from the pneumatic regulator to the actuator, it passes through this long pneumatic tube and a small pipe. The pneumatic air takes some time to travel from regulator to actuator because of air resistance and inertance. Hence, in this thesis, air resistance and inertance are modeled to estimate the phase shift of the signals and then to external forces acting on the actuator. Here we provide a 10 HZ sinusoidal signal to SPA. The pneumatic signals are measured near regulator P_{reg}, then near the actuator P_{act}. The obtained pressure signal in the time domain signal is converted into the frequency domain for further analysis. The phase shift is obtained around 10 Hz, as it is the dominant frequency for the signal. The obtained phase shifts are in radians.

Software:
We use the Matlab Simulink for data collection. Simulink controls pneumatic regulators and pressure sensors and has a data inspector displaying input and output signals. This feature helps to understand the relationship between different signals. Next, simulink auto generates C++ code and compiles the code in Arduino. The obtained time domain signal is exported to Matlab for further data analysis.

3.5.1 Experiments

This subsection describes the experiments conducted for characterization and validation experiments. During the characterization experiments, we restricted expansion using hands to validate the thesis. The stand, as shown in Figure 3.2 (11) was embedded with a load cell in order to measure experimental forces for the validation experiments. Here, we use second Arduino Uno to interface with load cell .

3.5.2 Characterization experiments

We conduct characterization experiments to validate the concept mentioned in the Literature review 2. Here, two different tests are conducted and compared. In the first test, the soft pneumatic actuator expands freely. This test is called the Free expansion. Next, the actuator is blocked. This test is called the Constrained expansion test.

According to the concept the phase shift obtained of Free expansion should be greater than the Constrained expansion. As we know from the hypothesis Figure 2.3 (a), when the actuator is blocked, the volume of the actuator is constrained. Hence the phase shift of the input sinusoidal signal reduces compared to free expansion. Here, five samples were taken for each case (Constrained expansion and Free expansion) where the pressure was increased from 0.2 to 0.5 bar with a 0.05 bar step increase.

3.5.3 Force tests

Here, load cell setup is used to constrain the actuator expansion. The load cell measures the experimental force. Here, five samples were taken for each case where the pressure was increased from 0.2 to 0.5 bar with a 0.05 bar step increase. Next, multiple chambers were used to validate the hypothesis. Since, load cell calibration were inaccurate. In this thesis, we use calibrated weight to validate the potential of SPA. A detailed validation experiments are explained in appendix. Next a linear regression model is created to estimate correlation between phase shifts and load cell forces. Here, chamber 1 is used for training the linear regression. We carried out a first order linear regression.

4 Results

This chapter describe results obtained in experiments. At first, characterization experimental results are presented, followed by force tests.

4.1 Control system results

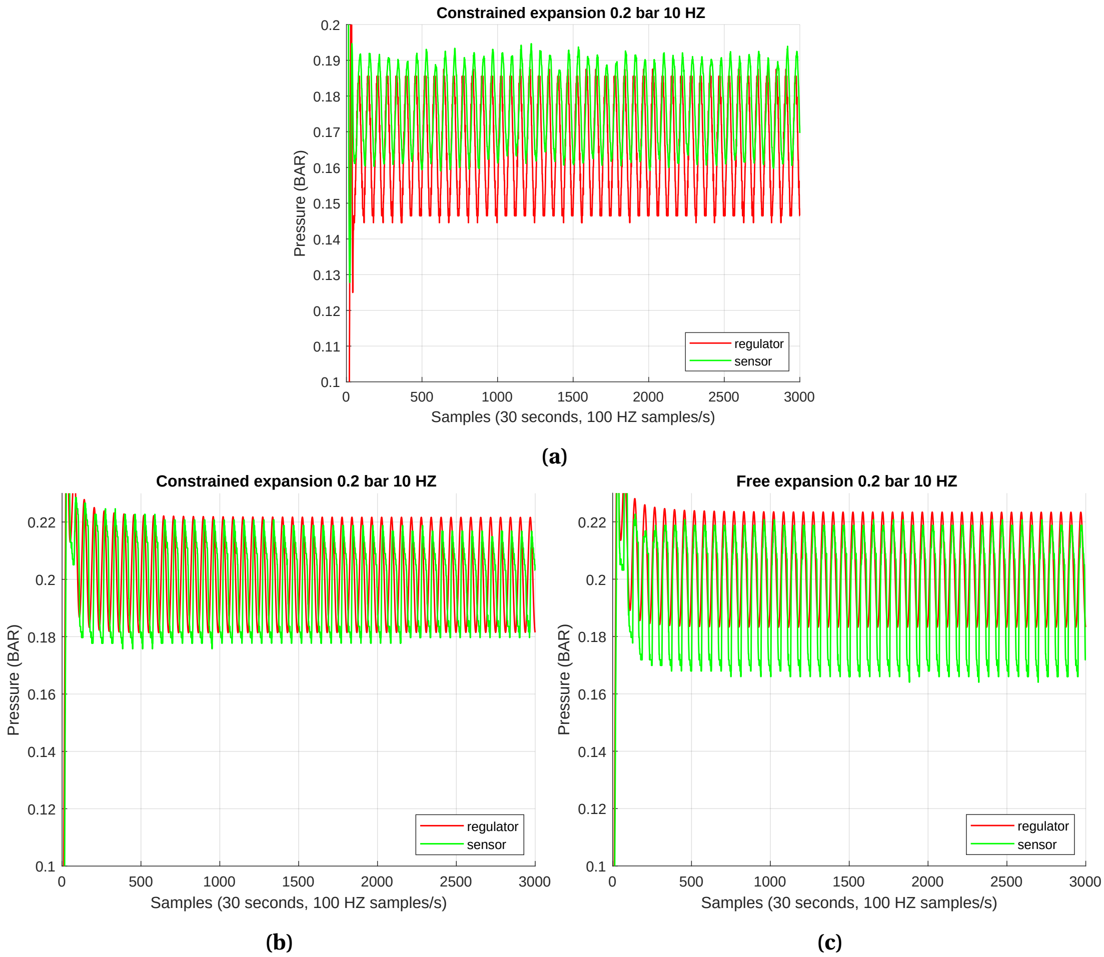

Figure 4.1: (a) Original system (b) Constrained expansion time domain analysis (c) Free expansion time domain analysis

The results of feedback loop is shown in Figure 4.1 (a,b) where (a) represents original signal and (b) represents feedback loop signal. This feedback loop ensure that the actuator receives optimal pressure input, to measure phase shift with respect to experimental forces.

4.2 Characterization Experiment results

Results shown here correspond to the single-chamber actuation of the SPA. A sinusoidal pressure signal with a frequency of 10 Hz and pressure variation of 0.04 bar was applied to the actuator. Figure 4.1 (b,c) shows the outcome of characterization experiments carried out at an amplitude of 0.2 bar in the time domain. Figures 4.2(a, b) are the results of the frequency-domain analysis.

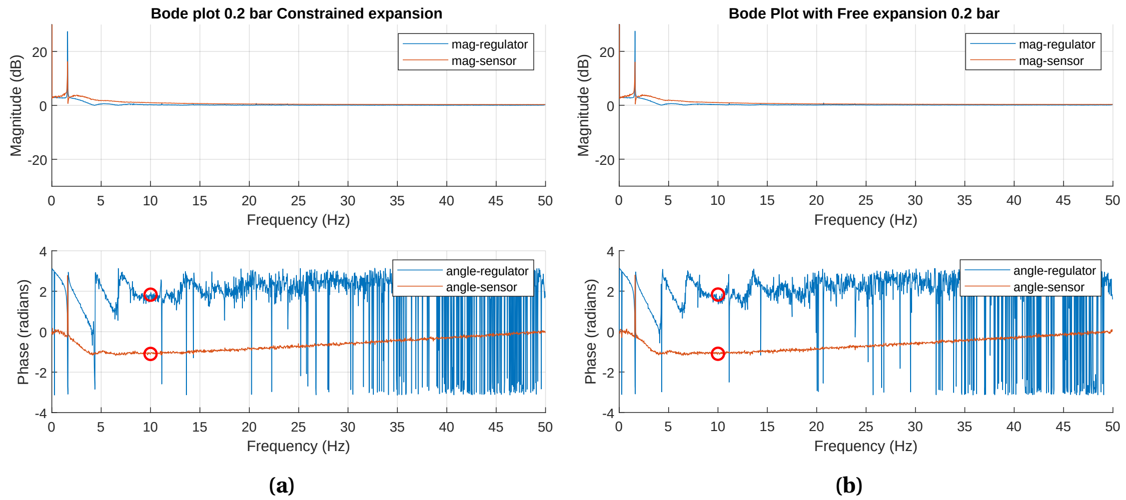

Figure 4.2: (a) Constrained expansion frequency domain analysis (b) Free expansion frequency domain analysis

These experiments were done over 30 seconds with a sampling frequency of 100 Hz. The time domain analysis is shown in Figures 4.1 (b,c), where the x-axis represents data points while the y-axis represents pressure in bar. The red signal represents the pressure sensor near the regulator while the green signal represents the pressure sensor near the actuator. First, an impulse response is observed for first 100 samples, followed by a sinusoidal signal. Frequency domain analysis is shown in Figures 4.2 (a, b) by bode plots for the signals acquired in the cases of constrained expansion and free expansion. Magnitude is expressed in decibel scale whereas the phase plot has been done in radian. The identified dominant frequency of the signal is marked with red circles in the bode plot. Long blue line in bode phase plot represent signal noises at their specific frequencies. A peak is seen at 3 Hz in magnitude plot.

Figure 4.3 (a,b) depicts a relationship between mean phase shift and input pressure. Here the mean phase shift is measured between two pressure sensors, one placed near actuator and one near the regulator. The data is presented for two conditions: Free expansion (blue line) and constrained expansion (red line). Here discrete measurements were taken at seven pressure points ranging from 0.2 bar to 0.5 bar, with increments of 0.05 bar and each pressure points were sampled five times. Figure 4.3 (a) depicts the mean phase shifts of characterization experiments. For better clarity data points are linked with solid lines. The bars depict mean phase shift, while the error bars (yellow and purple marks) represents standard deviation. From this graph one can see that with an increase in pressure, the phase shift increases. In Figure 4.3 (a,b) a significant change is seen in phase shift during the first rapid expansion phase, from 0.2 bar - 0.3 bar. specifically, at 0.25 bar constrained expansion has higher phase shift compared to free expansion. Next, in normal expansion phase, between 0.3 -0.4 bar, the phase shift of free and constrained expansion are almost similar. Significant changes are seen second rapid expansion phase, between 0.4 bar and 0.5 bar.

Figure 4.3 (c,d) outlines the pressure variations from the single pressure sensor located near the actuator. Pressure of 0.2 bar is used as a reference, and phase shift is measured relative to this value. Similar to other experiments, Phase shift measurements were taken at seven discrete pressure points ranging from 0.2 bar to 0.5 bar with increments of 0.05 bar and each pressure points were sampled five times. In general, the variations in phase shift increases with pressure. Figure 4.4 (a) depicts a relationship between phase shift and input pressure. Here the phase shift is measured between two pressure sensors, one placed near actuator and one

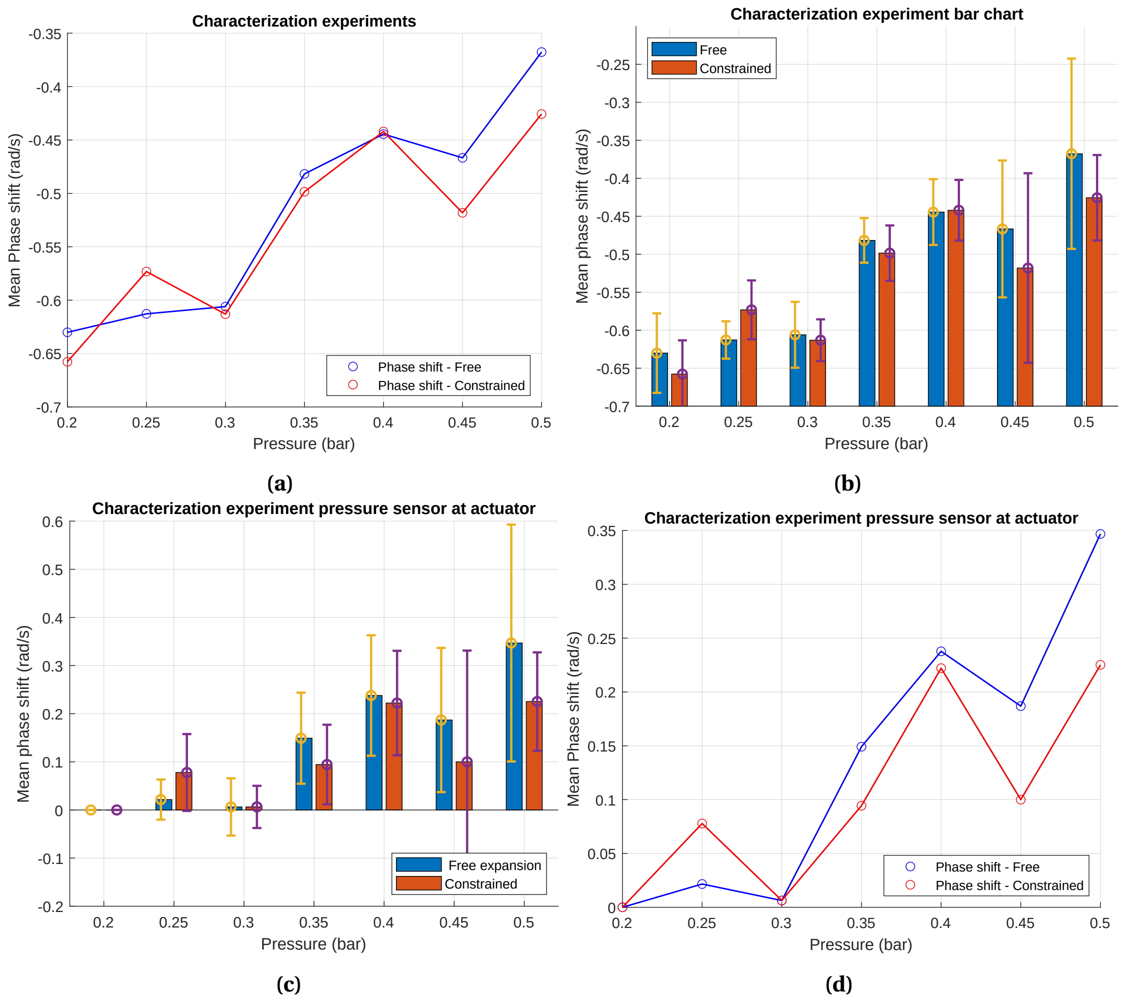

Figure 4.3: (a) Characterization experiment pressure vs phase shift (b) Graphical representation of characterization experiment (c) Influence of pressure in phase shift (d) Graphical representation of influence of pressure in phase shift.

near the regulator. Here the presented data represents constrained expansion of four different chambers. Phase shift measurements were taken at seven discrete pressure points ranging from 0.2 bar to 0.5 bar with increments of 0.05 bar and each pressure points were sampled five times. Next for better understanding of results, the average phase shift measured at 0.2 bar was subtracted from all the data points. This was performed to normalize this dataset and exhibit trends or relative changes in the dataset. Data are reported as bar plot with bars showing means, error bars show standard deviation determined through five samples per pressure point

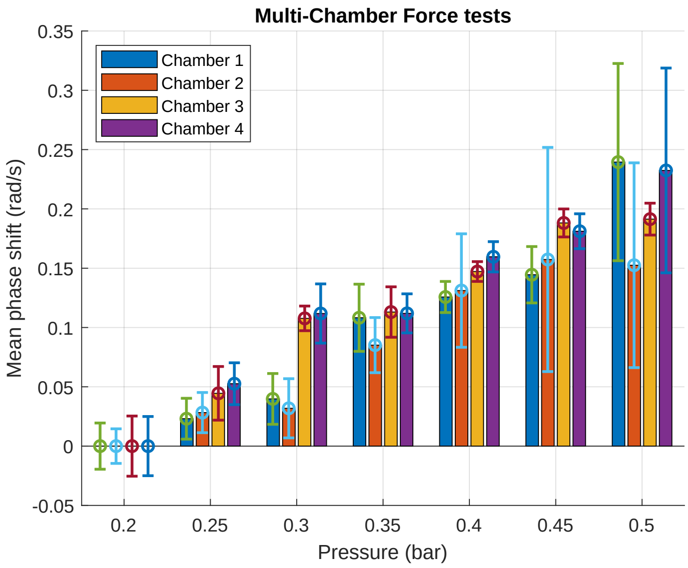

(a)

Figure 4.4: (a) Pressure vs phase shift on constrained condition for different chambers and actuators

4.3 Force test Results

The hypothesis section (3.2) was further verified with the help of experimentally measured forces. Figure 4.5(a) shows the experimental forces of multiple chambers, Chamber 1 has a maximum force of 0.21 N at 0.5 bar pressure. Figure 4.5(b) shows the mean phase shift in the case of multiple actuators. Here the presented data represents constrained expansion of four different chambers. Phase shift measurements were taken at seven discrete pressure points ranging from 0.2 bar to 0.5 bar with increments of 0.05 bar and each pressure points were sampled five times. Figure 4.5(c) depicts the linear regression analysis. The blue line represents the training data for Chamber 1, for which five samples were taken at each pressure point and their mean values were plotted. The black line plots the simple linear regression model fitted on the training data. Circles on the black line mark the estimated forces for the validation data. The red line represents the validation data. New set of data's were taken for validation, where each pressure points were sampled five times. For each pressure point, the mean estimated force and phase shift are also marked with encircled points. The horizontal error bars describe the standard deviation of the phase shift with respect to the pressure points, while the vertical ones stand for the standard deviations of the load cell force measurements.

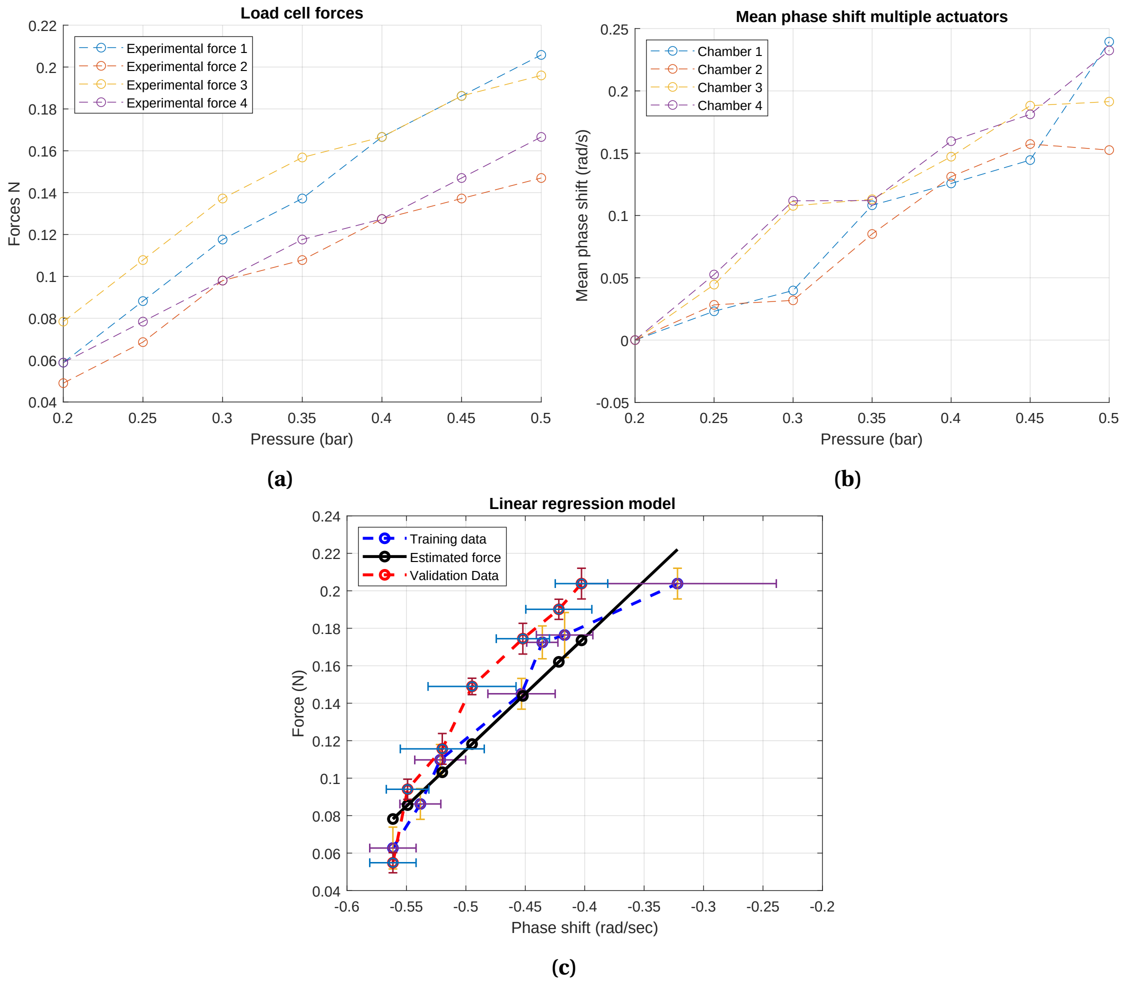

Figure 4.5: (a) Experimental forces (b) Mean phase shift (c) Linear regression

5 Discussions

Figure 4.1 (b,c) illustrates the time-domain analysis of the characterization experiments. These experiments investigate the relationship between pressure, volume, and phase shift by analyzing the free and constrained expansion of the soft pneumatic actuator (SPA). The hypothesis suggested by [10] Figure 2.3 (a) was such that under constrained expansion the actuator had a quicker rate of change of frequency as depicted by red ramp in the figure, though no such trend on frequency variation resulted from time domain data in Figure 4.1 (b) . This could be because of variety of reasons. First, the fiber-reinforced SPA used in the experiment is six times smaller compared to the SPA pack mentioned in the hypothesis. Secondly, here we use constant pressure pneumatic supply system (PSS) rather than the constant flow PSS as pointed out. As a result, a modified hypothesis in section (3.2) was developed based on [13] and developed in this thesis. This new formulated hypothesis was used to examine the relationship between pressure, volume, phase shift using frequency domain analysis.

In frequency domain analysis as shown in Figure 4.2 (a,b), the dominant phase shifts have been highlighted using a red circle. The variations in phase shifts were instrumental in estimating the external forces acting on the actuator. These phase shifts variations are clearly mentioned in Figure 4.3 (a,b). Next, in the second rapid expansion phase, starting from 0.4 bar to 0.5 bar phase shifts are clearly seen. Here, larger phase shift are seen in free expansions compared to constrained expansion. This aligns with the hypothesis. This suggest that, higher pressure produces higher external force, in constrained case, higher volumetric changes happen, which produces significant change phase shift. Hence, the difference in phase shift is more clearer with higher input pressure. However, at 0.25 bar due to rapid expansion and insufficient forces, constrained expansion shows abnormalities in phase shifts. In Figure 4.3 (b) the error bars overlap for both free and constrained expansion showing that the data are reliable. From these results we conclude that free expansion exhibits a greater phase shift compared to constrained expansion as a function of pressure. Next, the Figure 4.3 (c,d) represents phase shift of the pressure sensor near the actuator. This analysis was conducted to understand the influence of pressure in phase shifts. The phase shift increases with respect to pressure. Higher phase shifts are seen in second rapid expansion. We conclude that, phase shift increases with increasing pressure.

Figure 4.5 (b) depicts the relationship between pressure and phase shifts in constrained condition of four different chambers. The non linearities of SPA are clearly visible in this bar chart. As we can see chamber 1 and chamber 4 has maximum mean phase shift. Which is reflected in 4.5 (b). But chamber 1 and 3 has maximum experimental forces. We conclude that there is a nonlinear relation between phase shift and experimental forces. Among the two, chamber 3 is has maximum experimental force compared to chamber 4 as shown in Figure 4.5 (a). However, Chamber 4 shows higher mean phase shift than chamber 3 as shown in Figure 4.5 (b).This indicates that, no meaningful relationship can be obtained between phase shift and experimental forces. This graph in Figure 4.5 (a,b) highlights the nonlinear relationship between the experimental force and phase shifts, the experimental forces has smooth curve whereas the phase shifts shows similar trend. But both the graphs has similar upward trend. It is evident from these graphs, that higher pressure has higher experimental forces and higher phase shifts for all the chambers. These results suggest that there exist a similar trend between the external forces and phase shifts.

A linear regression model was used to establish a relationship between experimental forces and phase shift. It is shown in Figure 4.5 (c).The RMSE root mean square error is 0.024 N for force estimation. The mean phase shift of training data is 0.32 rad/s while it is 0.4 rad/s for the validation data at maximum pressure. These are slight differences are due to measurement noises. This linear regression is a chamber-specific model.

6 Conclusions and Recommendations

6.1 Conclusions

This thesis aimed to establish a relationship between pressure, volume and phase shifts of SPA. Initially, hypothesis proposed in the literature review was tested, suggesting that during free expansion, the frequency between the pressure sensors would be lower compared to the constrained expansion. However, this hypothesis was not feasible for fibre reinforced SPA's. Since the fibre reinforced SPA is six times smaller than the SPA pack, as well as it uses constant pressure Pneumatic Supply system. So, an alternative approach based on phase shift in frequency domain were explored.

In this thesis, we introduced a new hypothesis based on phase shifts. We observed that during free expansion, the phase shift between pressure sensors was higher compared to constrained expansion. Furthermore, we assumed that, phase shift reduction in constrained condition, corresponds to restrictions in actuator's volume expansion. To validate this hypothesis, series of characterization experiments were conducted. These experiments conforms a direct relationship between pressure, volume and phase shifts. The results indicate free expansion has higher phase shift compared to constrained expansion, with significant difference at higher points. Additionally, we absorbed that, increase in pressure leads to corresponding increase in phase shift. Additionally, further analysis revealed that because of non-linear behavior in actuators, external forces produced by the chambers are unique. Furthermore, a simple linear regression model was performed based on chamber one to establish a relationship between external forces and phase shifts. The model performs well with a root mean square error of 0.024 N.

In summary, the experimental results show a strong correlation between phase shift, external forces, and the change in volume of the soft pneumatic actuator. Furthermore, the nonlinear behavior of the soft actuators leads to variations in external forces, which are mirrored in the corresponding phase shifts. Thus, this thesis establishes a clear relationship between pressure, phase shift, and the external forces acting on the soft pneumatic actuator. Additionally, a simple linear regression model was developed, achieving a root mean square error (RMSE) of 0.024 N.

6.2 Recommendations

This thesis is a pilot study to estimate external forces acting on SPA using external pressure sensors. So, single chamber activation is activation is considered. Further, this work can be expanded to 2 chamber activation and 3 chamber estimation. Internal dynamics of SPA varies with two chamber and three chamber activation. Few modeling parameter has to be changed to obtain results.

In simulink Matlab, interfacing two different load cell and differential pressure sensor was not possible. Since they both worked in different frequencies. So, Robot operating system based model is preferred. Which would be faster and optimal to interface all sensing and control parameters.

High resolution and low signal to noise ratio sensors are preferred to obtain more precise and accuracy estimation of SPA. Here high resolution sensors were used but the signal to noise ratio was much higher. The frequency of sensor was reduced to obtain better accuracy.

A lumped parameter model is recommended for estimating external forces acting on the actuator. It will provide a general method to estimate forces irrespective of actuators, since actuators are non linear. Next, combing the lumped parameter approach with machine learning model would provide better accuracy and precision.

References

[1] M. Wildan Gifari et al. 'A review on recent advances in soft surgical robots for endoscopic applications'. In: *The International Journal of Medical Robotics and Computer Assisted Surgery* (Oct. 2019), e2010.

[2] Ali Shiva et al. 'Elasticity Versus Hyperelasticity Considerations in Quasistatic Modeling of a Soft Finger-Like Robotic Appendage for Real-Time Position and Force Estimation'. In: *Soft Robotics* 6.2 (Apr. 2019), pp. 228–249.

[3] Seung-Hwa Lee et al. 'Technical skills and training of upper gastrointestinal endoscopy for new beginners'. In: *World Journal of Gastroenterology: WJG* 21.3 (2015), p. 759.

[4] Yanheng Zhang et al. 'A Study on the Control of a Sensorless Pneumatic Joint Using Predictive Control Method'. In: *IEEE Access* 7 (2019), pp. 59923–59932.

[5] Iris De Falco, Matteo Cianchetti and Arianna Menciassi. 'STIFF-FLOP surgical manipulator: design and preliminary motion evaluation'. In: *Proc. 4th Workshop Computer/Robot Assisted Surgery (CRAS)*. 2014, pp. 131–134.

[6] LIN Yuanxiang. 'DESIGN OF PNEUMATIC SOFT SURGICAL ROBOT FOR ENDOSCOPIC NOTES AND MIS APPLICATION WITH REDUCED SIZE'. In: (Dec. 2019).

[7] Yoeko Xavier Mak et al. 'Adaptive control of a soft pneumatic actuator using experimental characterization data'. In: *Frontiers in Robotics and AI* 10 (15th Mar. 2023), p. 1056118.

[8] J. Fras et al. 'New STIFF-FLOP module construction idea for improved actuation and sensing'. In: *2015 IEEE International Conference on Robotics and Automation (ICRA)*. 2015 IEEE International Conference on Robotics and Automation (ICRA). Seattle, WA, USA: IEEE, May 2015, pp. 2901–2906.

[9] Liangliang Wang and Zheng Wang. 'Mechanoreception for Soft Robots via Intuitive Body Cues'. In: *Soft Robotics* 7.2 (1st Apr. 2020), pp. 198–217.

[10] Sagar Joshi and Jamie Paik. 'Sensorless force and displacement estimation in soft actuators'. In: *Soft Matter* 19.14 (2023), pp. 2554–2563.

[11] Matteo Cianchetti et al. 'STIFF-FLOP surgical manipulator: Mechanical design and experimental characterization of the single module'. In: *2013 IEEE/RSJ International Conference on Intelligent Robots and Systems*. 2013 IEEE/RSJ International Conference on Intelligent Robots and Systems (IROS 2013). Tokyo: IEEE, Nov. 2013, pp. 3576–3581.

[12] Sagar Joshi and Jamie Paik. 'Pneumatic Supply System Parameter Optimization for Soft Actuators'. In: *Soft Robotics* 8.2 (1st Apr. 2021), pp. 152–163.

[13] Eunok Jung. 'A Mathematical Model of Valveless Pumping: A Lumped Model with Time-Dependent Compliance, Resistance, and Inertia'. In: *Bulletin of Mathematical Biology* 69.7 (Oct. 2007), pp. 2181–2198.

[14] Wenjie Lai et al. 'Distal End Force Sensing with Optical Fiber Bragg Gratings for Tendon-Sheath Mechanisms in Flexible Endoscopic Robots'. In: *2018 IEEE International Conference on Robotics and Automation (ICRA)*. 2018 IEEE International Conference on Robotics and Automation (ICRA). Brisbane, QLD: IEEE, May 2018, pp. 5349–5255.

[15] Wenjie Lai et al. 'Force Sensing With 1 mm Fiber Bragg Gratings for Flexible Endoscopic Surgical Robots'. In: *IEEE/ASME Transactions on Mechatronics* 25.1 (Feb. 2020), pp. 371–382.

[16] Adrita Bima ADI. 'DEVELOPMENT OF A 3D-PRINTEDANGLE SENSORFORFEEDBACKINSOFTROBOTIC APPLICATIONS'. In: (Feb. 2021).

A Appendix

A.1 Limitations of current sensors

A wide variety of sensors can accomplish these tasks. Conventional sensors are built with standard shapes and sizes, which may not fit into the endoscopic module. Moreover, micro-sized sensors are expensive and MRI incompetent. Hence, the few options are optical fiber-based sensors, customized sensors specifically built to meet all the requirements, and external pressure sensors.

A.1.1 Fibre Bragg sensor

Fibre Bragg (FBG) is an optical sensor that uses light refraction to identify temperature or strain changes. Here, UV light is used to alter the core of the fiber. [14]

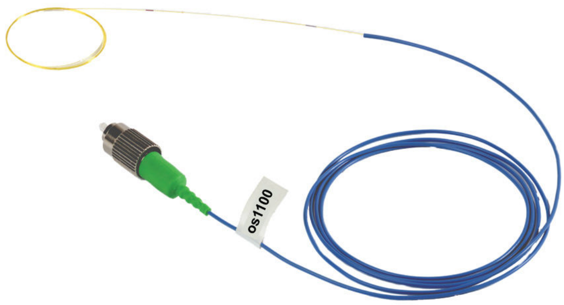

Figure A.1: Fibre bragg grating

FBG is an optical component inside an optical fiber. It produces periodic variations in the refractive index of the fiber core; it refracts a particular band of light, which shifts in response to variations due to temperature or strain. The central wavelength is called a Bragg wavelength. Bragg wavelength changes when optical fiber is exposed to a change in temperature and stain. When optical fiber encounters a change in temperature, it expands or contracts, which influences the Bragg wavelength. Concerning strain, when the optical fiber expands and contracts, it influences the refraction of light [15]. Similarly, when the FBG is stretched or compressed, the refractive index changes, and strain can be measured.
The Fibre Bragg sensor is highly efficient and accurate. Since it is a non-ferromagnetic material, it is MRI-competent. It is 1 mm in diameter so that it would be better for this application. However, it also has its drawbacks. It is expensive as it requires a complex manufacturing process. It requires precise alignment with the soft pneumatic actuator (spa) to measure accurate strain. It is susceptible to vibration and noise. So, a SPA with FBG sensors would produce inaccurate results. Next, the refracted wave needs an optical interrogator to read and analyze the refracted wavelength. The optical interrogator is highly expensive, and the data interpretation and calibration of FBG are time-consuming [14]. Subsequently, since the optical fiber expands due to temperature changes, it might influence the accuracy of external forces acting on the end-effector.
Moreover, fiber Bragg grating is expensive. Sensor mounting is challenging, and testing across different actuators is time-consuming. The sensor also reacts to changes in temperature. Hence, it is not an ideal sensor for SPA applications.

A.1.2 3D printed sensor

A customisable sensor can be a better alternative for these requirements, where sensors of specified shape, size, and material can be fabricated and tested.

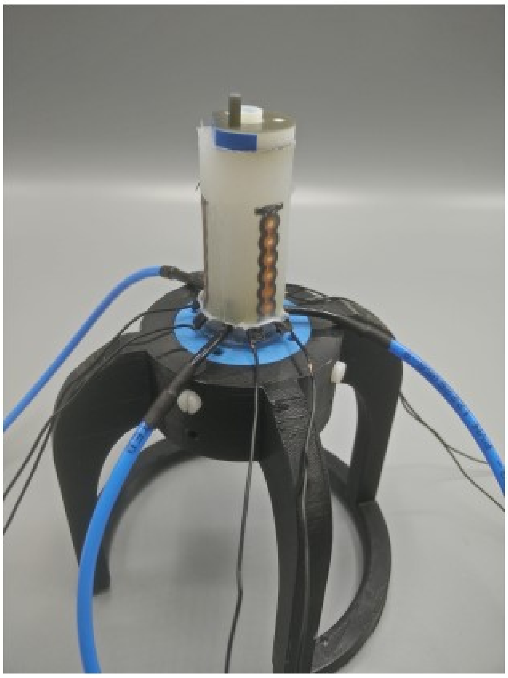

Figure A.2: 3D printed sensor

At the University of Twente, customized 3D-printed resistive length sensors were developed specifically for SPA. This research used fused deposition modeling (FDM) to print the sensor. Here, conductive and non-conductive thermoplastic polyurethane were used as sensor material [16].
A resistive strain gauge was fabricated, which elongates with the chambers in response to applied pressure. The spiral brown material seen in the image is the resistive strain gauge. In this research, a downsized STIFF-FLOP module was fabricated with a resistive strain gauge embedded in between them.
Eco-flex 0030 and Dragon Skin 10 were used for fabrication. The sensors are placed between the chambers, spaced radially equally beside the pneumatic chamber. The figure depicts three resistive strain gauges placed parallel to each chamber. Here, the change in resistance is proportional to the bending moment of SPA.
The experiments indicate that sensors increase the stiffness of the endoscope, reducing achievable bending moment by more than 50% . Additionally, The maximum pressure decreases from 0.43 bar to 0.3 bar, limiting the endoscope's potential and the maximum bending angle. This research concludes that the nonlinearity of the material and rate-dependent hysteresis leads to inaccurate, less precise, and non repeatable sensor measurements [16].

Therefore, placing sensors directly on the end effector limits the actuator's efficiency and results in inaccurate sensor measurements. This research focuses on an alternate approach to using external pressure sensors to estimate external forces acting on the actuator.

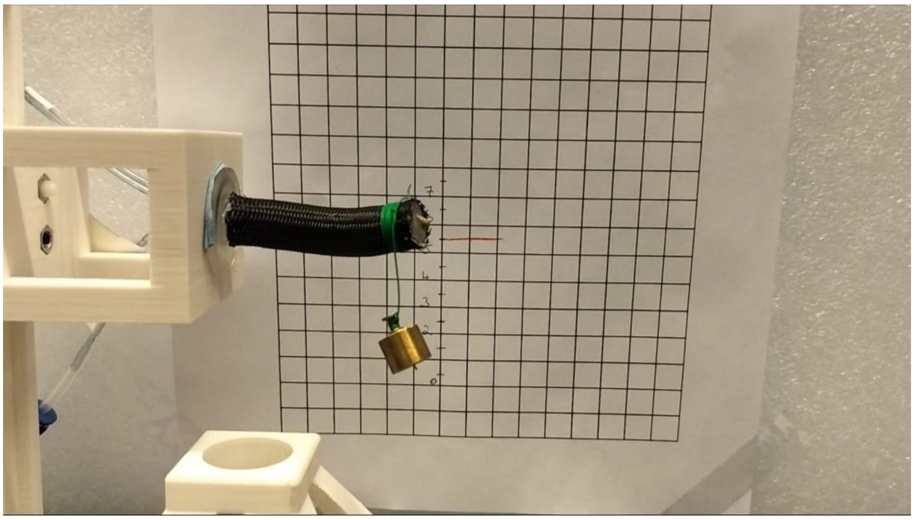

Figure A.3: Force calibration

A.2 Force calibration

Load cell calibration is essential for measuring external force exerted by the actuator. In this experiment, we use parallel beam load cell, to identify retroflex forces exerted by the SPA. Calibration was necessary because initially, the force sensors were providing faulty results. We used calibrated weights to verify the load cell calibration. As shown in the Figure A.3 20 g of calibrated weight was attached to the SPA. Initially, in no load, the position of the SPA is marked and it is represented by the red line in the image. Next, 20 g of weight was tied to the SPA, deforms the SPA. However, the SPA returned to its original position upon applying a maximum pressure of 0.5 bar. Through these experiments we concluded that fibre-reinforced SPA can exert a maximum force of 0.21 N. Based on this ground truth value, we set up the ADC to enable us to have accurate measurements of forces.